ACADEMIC PRESS

Available online at www.sciencedirect.com
SCIENCE DIRECT®

Journal of Sound and Vibration 260 (2003) 195–212

JOURNAL OF SOUND AND VIBRATION

www.elsevier.com/locate/jsvi

A dynamic model to determine vibrations in involute helical gears

A. Andersson, L. Vedmar*

Department of Machine Elements, Lund Institute of Technology, P.O. Box 118, SE-221 00 Lund, Sweden

Received 2 January 2002; accepted 15 April 2002

Abstract

A method to determine the dynamic load between two rotating elastic helical gears is presented. The stiffness of the gear teeth is calculated using the finite element method and includes the contribution from the elliptic distributed tooth load. To make sure that the new incoming contacts which are the main excitation source are properly simulated, the necessary deformation of the gears is determined by using the true geometry and positions of the gears for every time step of the dynamic calculation. This allows the contact to be positioned outside the plane of action. A numerical example is presented with figures that show the behaviour of the dynamic transmission error as well as the variation of the contact pressure due to the dynamic load for different rotational speeds.

1. Introduction

To design power transmission systems, it is essential to understand the dynamic behaviour of gears. In the literature, many studies of the dynamic behaviour of gear systems can be found. In the earliest analytical studies concerning the dynamic force on a gear, the gear was modelled as a mass–spring system with a constant mesh stiffness. During the years, more advanced and accurate models have been presented. An extensive review of the literature concerning mathematical models used in gear dynamics until 1988 was given by Özgüven and Houser [1].

Analysing helical gears is more complicated than analysing spur gears due to the oblique line of contact of the helical gears. Early experiments on the dynamic factors for both spur and helical gears were carried out by Houser and Seireg [2]. However, the measurements were limited to rotational speeds away from resonance.

*Corresponding author. Fax: +46-46-222-85-04.
E-mail address: lars.vedmar@mel.lth.se (L. Vedmar).

0022-460X/03/$ - see front matter
PII: S0022-460X(02)00920-3

The tooth stiffness is treated in different ways in the theoretical dynamic models of gears found in the literature. In the simpler models, the gear mesh stiffness is assumed to be constant. Also frequently used in the literature are the rough approximations of using a rectangular stiffness variation to represent a spur gear and a sinusoidal stiffness variation to represent a helical gear, see for example Ref. [3]. Umezawa et al. [4] developed an approximate function of the stiffness of a helical tooth pair based on a finite difference analysis of a rack-shaped cantilever plate with finite width. Cai [5] modified this function to include the effect of the tooth numbers and the addendum modification coefficients. However, by using these approximate functions, no information concerning the load distribution along the face width can be obtained and the influence of the magnitude of the load on the tooth stiffness is neglected. In a later report, Umezawa et al. [6] used an effect function considering the bending deformation of the gear tooth and an effect function considering the compressive deformation to describe the gear tooth deformation. Numerical solutions for several kinds of tooth surface deviations were presented and compared with experimental results.

Most dynamic models of helical gears presented in the literature, including those mentioned above, are models with a single degree of freedom. Additional degrees of freedom (d.o.f.) of the pinion and the gear can be included in order to analyse the gear motions. Blankenship and Singh [7] developed a model with six d.o.f. per gear. A reduced form of that model was presented by the same authors [8] where translations of the gear body normal to the line of action were neglected and consequently five d.o.f. per gear were used. Also in Kahraman [9] five d.o.f. per gear were used. In both Refs. [8,9] a constant mesh stiffness was used, thus making the parameters of the differential equation time invariant. The static transmission error was used as an excitation of the system. Velex and Maatar [10] introduced a six d.o.f. model for a single stage helical gear in order to analyse the influence of shape deviations and mounting errors on gear dynamics. Here, also the motor and the load with their connecting shafts were represented as inertias and stiffnesses.

In a series of papers, Honda [11–13], contact outside the plane of action was accounted for when obtaining the dynamic increment of the tooth load. To calculate the spring constant of the tooth-pair, the approximate function of Umezawa was adopted.

In most of the previous reports on gear dynamics, the contact between the gear teeth is prescribed to be positioned solely in the plane of action. Furthermore, the deformation of the gears is usually considered to be the transmission error, possibly reduced by the profile deviation from involute. These two assumptions will give rise to an abrupt transient loading of the gear teeth when a new tooth pair is about to enter the meshing region, at least if the profile deviation is less than the transmission error. A corresponding instantaneous unloading takes place when a tooth pair leaves the meshing region. Such a transient loading will give an incorrect influence on the dynamic response.

The main objective in the this paper is to present a method to determine the dynamic load in a helical gear set considering the actual positions of the contacts and the actual deformations of the gear teeth. By this method, the transient loading and unloading is avoided. In a geometrical analysis, the positions of the contacts, which may be positioned outside the plane of action, as well as the actual deformations of the gear teeth can be determined. This geometrical analysis is carried out every time the contact force changes, i.e., in every time increment in the dynamic simulation process. The deformations from the geometrical analysis are then used in order to determine the load distribution between the gear teeth.

Using this procedure of calculating the actual deformations from a geometrical analysis, the deformation and the contact force simultaneously start from zero when a new tooth pair comes into contact. As the meshing cycle proceeds, the load will continuously increase in correspondence to the deformation of the gear teeth. This way of loading the gear teeth will give a smoother and more realistic loading than if the load instantaneously starts to act on the gear teeth.

2. Dynamic model

The dynamic gear load will be affected not only by the gears themselves, but also by the connected parts. These parts are here represented by a one-degree-of-freedom system at each side of the gear set, each part being represented by a massless torsionally elastic shaft connected to a mass, see Fig. 1. The system is loaded with a torque at each side, M and Mz_g/z_p.

In a lubricated contact between two gear teeth the friction is small and will therefore give a very limited effect on the contact force. Due to the change in sliding directions at the pitch point, the friction could possibly contribute to the excitation of the vibrations. However, this disturbance will occur with the same frequency as the much more dominant meshing disturbance and the friction is therefore neglected. In order to give the vibration an opportunity to reach a steady state condition, some kind of damping has to be involved in the analysis. Here, the damping is assumed to originate from internal friction due to imperfect elasticity of the material. In such cases, the damping effect is low and there is therefore no need to treat the damping in a complicated manner. For that reason, the damping is here simply modelled as viscous damping, which is assumed to be present in the two subsystems at each side of the gear set and in the gears. The bearings, necessary to support the different parts in the model are assumed to be rigid. Consequently, the degrees of freedom considered in this study are the angular positions, φ_p, φ_g, φ_1 and φ_2, of the masses involved in the model.

To be able to calculate the instantaneous gear load, the instantaneous angular positions of the gears have to be known. These are given by the solution of the system of equations of motion, which can be written as

$$J_1\ddot{\varphi}_1 = M - c_1(\varphi_1 - \varphi_p) - d_1(\dot{\varphi}_1 - \dot{\varphi}_p), \tag{1}$$

$$J_p\ddot{\varphi}_p = c_1(\varphi_1 - \varphi_p) + d_1(\dot{\varphi}_1 - \dot{\varphi}_p) - M_{F,p} - M_{D,p}, \tag{2}$$

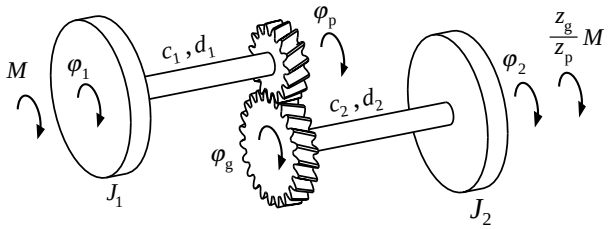

Fig. 1. Gear set.

$$J_g\ddot{\varphi}_g = -c_2(\varphi_g - \varphi_2) - d_2(\dot{\varphi}_g - \dot{\varphi}_2) - M_{F,g} - M_{D,g}, \tag{3}$$

$$J_2\ddot{\varphi}_2 = M\frac{z_g}{z_p} + c_2(\varphi_g - \varphi_2) + d_2(\dot{\varphi}_g - \dot{\varphi}_2), \tag{4}$$

where the torque contributions from the gear contact are given by $M_{F,p}$ and $M_{F,g}$, originating from the elastic deformation of the gears, and by $M_{D,p}$ and $M_{D,g}$, originating from the damping in the gears. The notation is defined in Appendix A.

Before the equations of motion can be solved, these torque contributions have to be expressed as functions of the angular positions of the pinion, φ_p, and the gear, φ_g, and, possibly, their derivatives. To be able to do this, the instantaneous load distribution between the gear teeth in mesh must be known for different combinations of φ_p and φ_g. For a specific combination, the load distribution can be calculated once the stiffnesses of the gears are known in all the simultaneous contact points. In this paper, the stiffness is calculated using the true geometry of the gears instead of using an assumed stiffness. This includes taking into account the deformation of the gears. In contradiction to the situation when the gears are assumed to be stiff, the contact between elastic gears takes place outside the plane of action at the beginning and at the end of the mesh. In addition, tooth profile errors or modifications also result in contact outside the plane of action. Consequently, before the stiffness in the simultaneous contact points can be determined, the positions of these points have to be determined.

3. Instant line of contact

If two infinitely stiff perfect involute helical gears are in contact with each other, the line of contact is a straight line in the plane that connects the two base cylinders tangentially, i.e., in the plane of action. For elastic gears, this contact line will be expanded to a contact area due to the local deformation in the contact. The width of this contact area depends on the shape of the gear teeth and the magnitude of the load and by that, the width will vary along the contact length. However, the contact width is very small compared to the contact length. Therefore, the load distribution across the contact, in a specific position along the contact line, is almost completely determined by the geometry of the gear teeth and the load intensity in that position only. This distribution is, of course, the elliptic Hertzian distribution. The centre points of these Hertzian contacts together form a curve that hereinafter will be called the instant line of contact.

The gear teeth considered in this study have an involute profile with a tip relief corresponding to the basic rack, see Fig. 2. The involute surface and the tip relief surface are described in detail by Vedmar [14]. When the connection between the tip relief and the tip surface is modelled as a sharp edge, a singularity will appear when calculating the deformation if the edge is in contact with the tooth flank of the other gear wheel. To avoid this, two different techniques can be used: (a) using a tip relief large enough to prevent the sharp edge from making contact, or (b) instead of the sharp edge applying a small tip rounding which does not prevent the contact but eliminates the singularity. Here, a tip rounding, which is defined by a circular arc in the transverse plane with a tangential junction with both the tip relief and the tip surface, is applied, see Fig. 2.

Fig. 3 shows the undeformed geometry of a tooth pair in an arbitrary transverse plane, which is defined by the axial non-dimensional coordinate ζ. The angular positions of the pinion and the

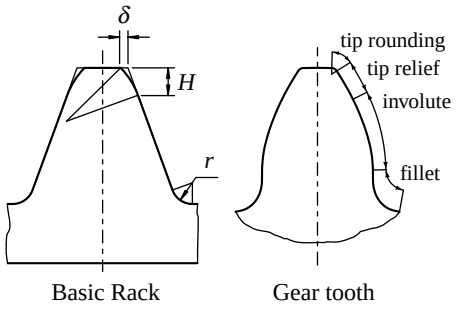

Fig. 2. Basic rack in the normal plane. Gear tooth profile in the transverse plane.

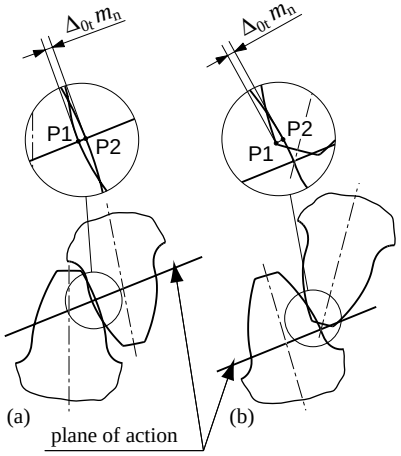

Fig. 3. Contact between two gears in the transverse plane for (a) an involute/involute contact and (b) an involute/tip rounding contact.

gear are φ_p and φ_g. In Fig. 3a both gear wheels have an involute profile at the contact while in Fig. 3b a tip rounding is in contact with an involute profile and thereby the contact is outside the plane of action. The appearing "overlap" along the common normal of the two tooth profiles corresponds to the necessary total deformation of the gear teeth. Two points, one on each gear flank, P1 and P2, can be found where the two gear flanks have the same normal in this transverse plane. These points are assumed to be the centre points of the Hertzian distribution and the distance between them along the common normal is $\Delta_{0t} m_n$. This distance can be calculated as a function of ζ provided that the positions of the pinion and the gear, φ_p and φ_g, are known. The points of contact in the different transverse planes together construct the line of contact. In the case of rigid bearings, the position of the instant line of contact is uniquely determined by the two angular co-ordinates φ_p and φ_g.

At a specific time in the numerical dynamic calculation, the angular positions of the pinion and the gear, φ_p and φ_g, are known. It is then trivial to calculate the points of contact in the interval between transverse planes where the involute surface of the pinion is in contact with the involute surface of the gear. In this interval, the line of contact is a straight line in the plane of action. Also in the interval between transverse planes where one involute surface is in contact with the tip

rounding, the point of contact can be determined explicitly. However, in the interval between transverse planes where one involute surface is in contact with the tip relief, the points of contact must be calculated using a numerical method.

4. Tooth deformation

To determine the load distribution along the line of contact, the elastic deformations of the tooth must be examined. When two helical gears are in contact, the load distribution across the line of contact is the elliptic distribution given by Hertz, see Fig. 4. In accordance with the principle of Saint-Venant, deformations relatively far away from the contacting area can be determined even if the local load distribution is not the correct one. Only the magnitude of the load must be correct. However, when studying the deformation in the near surrounding of the contact area, no such reference to the principle of Saint-Venant can be used to avoid using the correct distribution when loading the gears. Here, the deformation at the same point as where the load acts should be determined. When calculating the deformation, the gear flanks thereby have to be loaded with the correct load distribution, i.e., the elliptically distributed load. Using the finite element method to calculate the displacements therefore requires so many elements in the contacting area that the node forces in the contact together can approximate the elliptic load distribution. As the displacements must also be determined for different load positions on the tooth flank, there has to be a large number of nodes along the height of the tooth. Together with the fact that a helical gear must be modelled in three dimensions, the finite element mesh would have to be so fine that there would be considerable problems to solve the case on a computer today.

Fortunately, the load case in Fig. 4 can be substituted by a number of cases where the linear part of the displacement is separated from the non-linear contact displacement using an approach developed by Vedmar [14]. According to this approach, the load condition in Fig. 4 is divided into the first two load cases of Fig. 5. The magnitude of the point load is the same as the magnitude of the Hertzian load distribution. In the second load case of Fig. 5 a fixed border can be set in accordance with the principle of Saint-Venant, provided that the thickness h of the gear flank strip

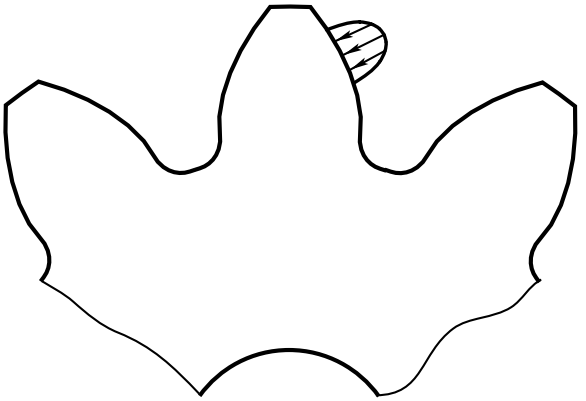

Fig. 4. Tooth load.

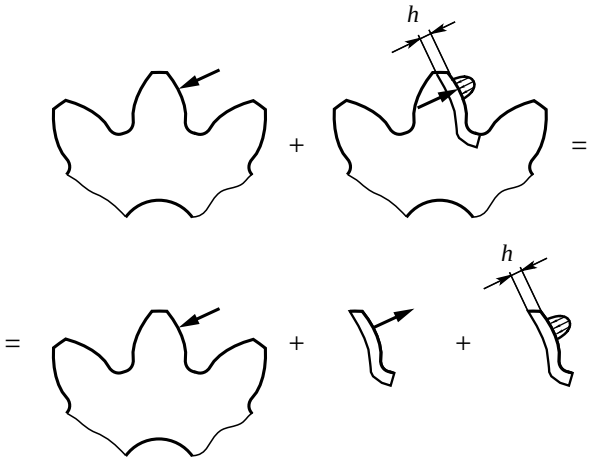

Fig. 5. Division into load cases.

is sufficiently large. After a final division, three load cases are obtained, see Fig. 5. The first two of these load cases together give the global deformation, which is proportional to the load applied. Global deformation here means all deformation except what the elliptic distributed contact load gives rise to between the surface and a point at the distance h from the surface. This missing part required to fully describe the deformation is obtained in the last load case in Fig. 5. This local contact deformation is non-linearly dependent on the magnitude of the load, since the extension of the Hertzian load depends on the magnitude of the load.

4.1. Global deformation

The global deformation is calculated using the finite element method. The two finite element models used are shown in Fig. 6. The elements used are 20-node three-dimensional isoparametric elements. A unit load was applied at each of the nodes on the gear flank, one at a time. The displacement at each node on the gear flank was then registered for each unit load.

Furthermore, to be able to calculate the load distribution later, the deformation at an arbitrary point on the line of contact due to a force applied in an other arbitrary point, also located on the line of contact must be calculated. This was done by interpolating between the distinct values from the finite element analysis and, based on those results, constructing approximate interpolation formulas. The influence function, i.e., the non-dimensional displacement in the direction normal to the surface at the point (η^*, τ, ζ) on the line of contact due to a unit force applied at the point $(\eta_F^*, \tau_F, \zeta_F)$, is named α. Here, the coordinate η^* (or η_F^*) is the distance between the common point of the tip rounding and the involute (neglecting the tip relief) and the point in question where the deformation is to be determined (or where the unit force is applied) along the symmetry line of the tooth in the current transverse plane. If the point in question is located on the tip rounding, the co-ordinate τ represents the angle to the current point from the common point of the tip rounding and the involute. If the point in question is on the involute surface, τ is 0. The

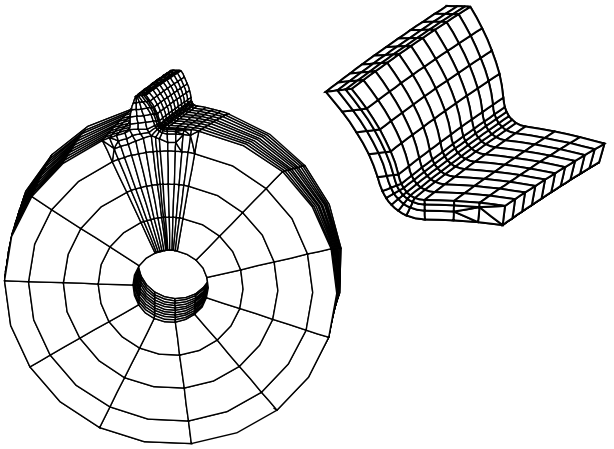

Fig. 6. Finite element mesh.

interpolation formula is constructed as

$$\alpha = \sqrt{\psi(\eta^*, \tau, \zeta)\psi(\eta_F^*, \tau_F, \zeta_F)} \cdot \Gamma(\eta^*, \eta_F^*, \zeta, \zeta_F), \tag{5}$$

where

$$\begin{aligned}\psi(\eta^*, \tau, \zeta) = {} & A_0 + A_1 e^{A_2\eta^*} + B_0\tau + (A_3 + A_4 e^{A_5\eta^*} + B_1\tau)e^{(A_6 + A_7\eta^*)\zeta} \\ & + (A_8 + A_9 e^{A_{10}\eta^*} + B_2\tau)e^{(A_{11} + A_{12}\eta^*)(b_0 - \zeta)},\end{aligned} \tag{6}$$

$$\Gamma(\eta^*, \eta_F^*, \zeta, \zeta_F) = e^{-(f(\eta^*, \eta_F^*, \zeta, \zeta_F))|\zeta - \zeta_F|^{C_9}}, \tag{7}$$

$$\begin{aligned}f(\eta^*, \eta_F^*, \zeta, \zeta_F) = {} & C_1 + C_2(\eta^* + \eta_F^*) + C_3\eta^*\eta_F^* + C_4(\eta^* + \eta_F^*)/(1 + (\zeta - \zeta_F)^2) \\ & + (C_5 + C_6(\eta^* + \eta_F^*) + C_7\eta^*\eta_F^*)(b_0 - \zeta - \zeta_F)^2 \\ & + C_8(\eta^* + \eta_F^*)\sqrt{\psi(\eta^*, \tau, \zeta)\psi(\eta_F^*, \tau_F, \zeta_F)}.\end{aligned} \tag{8}$$

Constants A, B, and C are calculated with a least-square method based on the results of the finite element analysis. In order to check the resemblance between the approximating formula, Eq. (5), and the values from the finite element analysis the relative deviation is studied. The relative deviation is here defined as

$$e_{rel} = (\alpha - \alpha^*)/\psi(\eta_F^*, \tau_F, \zeta_F), \tag{9}$$

i.e., the difference between the displacements calculated by the approximating formula, α, and the displacements from the finite element analysis, α^*, divided by the displacement at the point where the load is applied. The relative deviation is calculated for every value used to calculate the constants in Eqs. (6)–(8). The standard deviation of those data of relative deviations is an indicator of the resemblance.

4.2. Local deformation

The non-linear local deformation, which is the deformation between the tooth surface and the border at the depth h, due to the Hertzian contact pressure is calculated by using the formula derived by Weber and Banaschek [15]:

$$u_c = \frac{2(1-v^2)}{\pi E} q \left[\ln\left(\frac{h}{L} + \sqrt{1+\left(\frac{h}{L}\right)^2} \right) - \frac{v}{1-v}\left(\frac{h}{L}\right)^2 \left(\sqrt{1+\left(\frac{L}{h}\right)^2} - 1 \right) \right], \tag{10}$$

where q is the load intensity and $2L$ is the extension of the load, which is calculated as

$$L = \sqrt{\frac{4}{\pi}((1-v_p^2)/E_p + (1-v_g^2)/E_g) q \rho}, \quad \rho = \frac{\rho_p \rho_g}{\rho_p + \rho_g}. \tag{11}$$

5. Load distribution

For a certain position of the pinion, φ_p, and the gear, φ_g, the position of the instant line of contact can be calculated using the undeformed geometry of the gear wheels. This geometrical analysis also gives the total deformation of the gear teeth along the normal direction, which is necessary to overcome the "overlap", as a function of the coordinate ζ according to the first line in Eq. (12). The angle θ is the base cylinder helix angle. The total deformation along the normal direction at a specific ζ-co-ordinate can also be expressed by the sum of the global and the local deformations, as in the second line of Eq. (12):

$$\begin{aligned} u(\zeta) &= \Delta_{0l}(\zeta) m_n \cos\theta, \\ u(\zeta) &= \int_{\zeta_b}^{\zeta_e} \alpha(\zeta, \zeta_F) q(\zeta_F) \frac{m_n \, \mathrm{d}\zeta_F}{\cos\theta} + 2u_c(\zeta, q(\zeta)), \\ \alpha &= \alpha_p(\zeta, \zeta_F) + \alpha_g(\zeta, \zeta_F). \end{aligned} \tag{12}$$

The contact begins at the co-ordinate ζ_b and ends at the co-ordinate ζ_e. The co-ordinate ζ refers to the point of observation and the co-ordinate ζ_F refers to the loading point. The contact line was then discretised, whereby Eq. (12) is turned into a system of non-linear equations from which the load distribution $q(\zeta)$ can be solved using a numerical method.

When the load distribution is known, the torque due to the elastic deformation of the gears can be calculated from

$$M_{F,i} = \sum_{j=1}^{N} \int_{\zeta_{b,j}}^{\zeta_{e,j}} s_i(\zeta) q(\zeta) m_n \, \mathrm{d}\zeta, \quad i = p, g, \tag{13}$$

where $s(\zeta)$ is the moment arm which, if the contact is in the plane of action, is equal to the base radius. N is the number of simultaneous gear pairs in mesh. The damping force is assumed to be equally distributed along the instant line of contact and the base circle radius is adopted as the

moment arm. The torque due to damping can then be written as

$$M_{D,i} = d_{mesh}(\dot{\varphi}_p g_p + \dot{\varphi}_g g_g) g_i \sum_{j=1}^{N} (\zeta_{e,j} - \zeta_{b,j}), \quad i = p, g. \tag{14}$$

When the load distribution is known, the contact pressure along the line of contact can be calculated according to Hertz' theory as

$$p(\zeta) = \sqrt{\frac{q(\zeta)}{\pi((1 - v_p^2)/E_p + (1 - v_g^2)/E_g)\rho(\zeta)}}. \tag{15}$$

The load distribution and the extension of the contacts can now be inserted in Eqs. (13) and (14) to calculate the torque contributions due to the contact between the pinion and the gear. These torque contributions are inserted in Eqs. (2) and (3), and the system of differential equations can then be solved. Due to the complexity of the relation between the transmitted torque and the angular positions, a numerical solution technique has to be used.

6. Results

The method described can be used to calculate the variation of the load distribution along the face width, and thereby the variation of the gear contact load, as the gears rotate at a certain rotational speed under the influence of a driving and a braking torque. Although it would be, in some cases, highly interesting to study the variation of the contact load during start up or during another prescribed acceleration, the present study is restricted to the steady state condition. The forces calculated in such a condition have to be known to give a possibility to make a lifetime prediction of the gears when they are running at a normal, non-accelerating condition. Here, a gear set with the dimensions according to Table 1 has been analysed.

Table 1
Numerical data

Number of teeth	$z_p = 30$, $z_g = 47$
Normal module	$m_n = 3\,\text{mm}$
Face width	$b = 15\,\text{mm}$
Pressure angle	20°
Helix angle	$\beta = 10^\circ$
Basic rack fillet radius	$r = 0.35m_n$
Basic rack tip relief	$\delta = 0.015m_n$
Basic rack relief height	$H = 0.5m_n$
Tooth tip rounding radius	$0.05m_n$
Torque	$M = 100\,\text{Nm}$
Hub bore diameter	15 mm
External inertia	$J_1 = J_2 = 0.62\,\text{kgm}^2$
Shaft stiffness	$c_1 = c_2 = 984\,\text{Nm}$
Shaft damping	$d_1 = d_2 = 0.04\,\text{Nms}$
Normal backlash	$0.0725m_n$
Standard deviation of e_{rel}	0.02

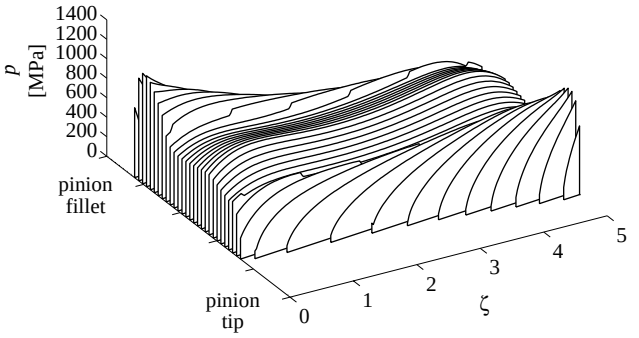

Fig. 7. Contact pressure, $\omega_p = 0$ rad/s.

First, consider the static case. The equilibrium equations can be obtained from Eqs. (1)–(4) by omitting the dynamic terms which contain $\dot{\varphi}$ or $\ddot{\varphi}$. During the meshing cycle, i.e., for different positions of the pinion, a gear tooth will be exposed to a load which will change throughout the mesh. This load is not uniformly distributed along the face width, which means that the load distribution $q(\zeta)$ will vary along the face width as well as throughout the mesh. The contact pressure distribution $p(\zeta)$, which depends on both the variation of the load distribution and the variation of the radii of curvature at the point of contact, will accordingly also vary along the face width as well as throughout the mesh. For each position of the pinion, the position of the line of contact for the current magnitude of the loading torque was determined. The line of contact was discretised into a number of portions (in the present study 200 portions gave satisfactory accuracy) and the load distribution was calculated by solving Eq. (12). To calculate the contact pressure in accordance with Eq. (15), the radii of curvature of the gear flanks in contact must also be known. These radii of curvature are obtained analytically or numerically depending on if the point of contact is on the involute, on the tip relief or on the tip rounding. Fig. 7 shows the contact pressure along the face width for the static case. Each slice in the waterfall diagram shows the instant contact pressure distribution for a certain angular position of the pinion, φ_p. The figure is plotted with 20 slices per pitch. At some slices, there appears a ruggedness of the pressure distribution at a certain ζ-co-ordinate. This ruggedness appears due to the discontinuity in the radius of curvature where the instant line of contact changes from being on the involute surface to being on the surface with tip relief. However, in practice the ruggedness will be somewhat smoother since in an interval along the line of contact, the Hertzian zone will cover part of both the involute profile and the tip relief profile. Any corresponding influence of the discontinuity in radius of curvature between the tip relief and the tip rounding cannot be observed in Fig. 7 since the tip relief in this case is large enough to prevent the tip rounding to get into contact.

When running the gear at a specific rotational speed, the gear teeth, due to oscillations, most often will be exposed to higher loads than what is the result from a strictly static analysis. This increased load can be crucial in the choice of gears and gear parameters, especially as some of the parameters will affect the dynamic behaviour of the gear set. The magnitude of the oscillations will here be quantified by the transmission error along the line of action,

$$TE = \varphi_p g_p + \varphi_g g_g. \tag{16}$$

The transmission error is zero in the case of unloaded and perfect involute gears. To show the dynamic influence, the transmission error can be compared with the static transmission error (*STE*), which is obtained by using the static solution of Eq. (16). The relationship between the transmission error and the load intensity that the gear teeth are exposed to is rather complex, see Eq. (12). Of course, this relationship varies due to the variation of stiffness at different instants of the meshing cycle. Furthermore, the relationship is affected by the size of the tip relief since the geometry and thereby Δ_{0t} then will be affected. In addition, the load intensity at a point is affected by the load distribution along the line of contact. However, principally a large transmission error implies a large load intensity. Consequently, intervals of rotational speeds that have a larger maximum transmission error imply that the gear teeth are exposed to a larger load intensity and they are thereby exposed to a higher stress in these intervals.

The system of differential equations, Eqs. (1)–(4), was solved numerically with a Runge–Kutta method for different rotational speeds. Due to the restriction given earlier, the calculation was interrupted when a steady state condition was reached. A flow chart of the computational procedure used when calculating the dynamic response for a specific rotational speed is shown in Fig. 8. By analysing the same gear set for different rotational speeds, the resonance speeds can be detected. In Fig. 9 the maximum value of the transmission error in a steady state is shown relative to the maximum value of the static transmission error, which in the current case is 30.5 μm. The main resonance due to parametric excitation is found at the rotational speed of $\omega_{p,crit} = 660$ rad/s. Additional resonance frequencies, also due to parametric excitation, appear at rotational speeds of $\omega_{p,crit}/2, \omega_{p,crit}/3, \ldots$.

With the damping coefficient $d_{mesh} = 100$ N s/m, the oscillations become so large that the minimum value of the transmission error of the steady state solution becomes negative in an interval of rotational speeds near the main resonance. This implies that the two gear wheels lose contact with each other, and possibly also that the gear wheels make contact at the backside of the gear teeth if the oscillations overcome the backlash. From an engineering point of view, the only interest concerning these intervals is how to avoid them. Therefore, in this study, the steady state solution was not examined further once it was concluded that the gear wheels lose contact with each other. Consequently, the interval of rotational speeds where tooth separation occurs is in Fig. 9 only indicated as a break in the graph. The magnitude of damping strongly affects the amplitude of the vibrations in the resonance regimes. However, the small magnitude of damping that is relevant here does not affect the position of the resonances, i.e., the rotational speeds where the oscillations become larger remain the same. With a damping coefficient of twice the size as before, $d_{mesh} = 200$ N s/m, the oscillations become smaller at the resonance speeds. The contact between the pinion and the gear is then maintained during the whole meshing cycle independently of the rotational speed.

When the gears rotate at a specific rotational speed, the variation of the transmission error can be studied as the gears rotate. The dynamic transmission error will oscillate around the static transmission error. Especially, the variation of the transmission error in a steady state during three pitches when the gears rotate at the second and the third resonance is shown in Fig. 10. The transmission error in Fig. 10 is normalised by division by the maximum static transmission error, and the static transmission error is shown as a reference. At the resonance frequencies, the number of oscillations during one pitch is the same as the ordinal number of the resonance.

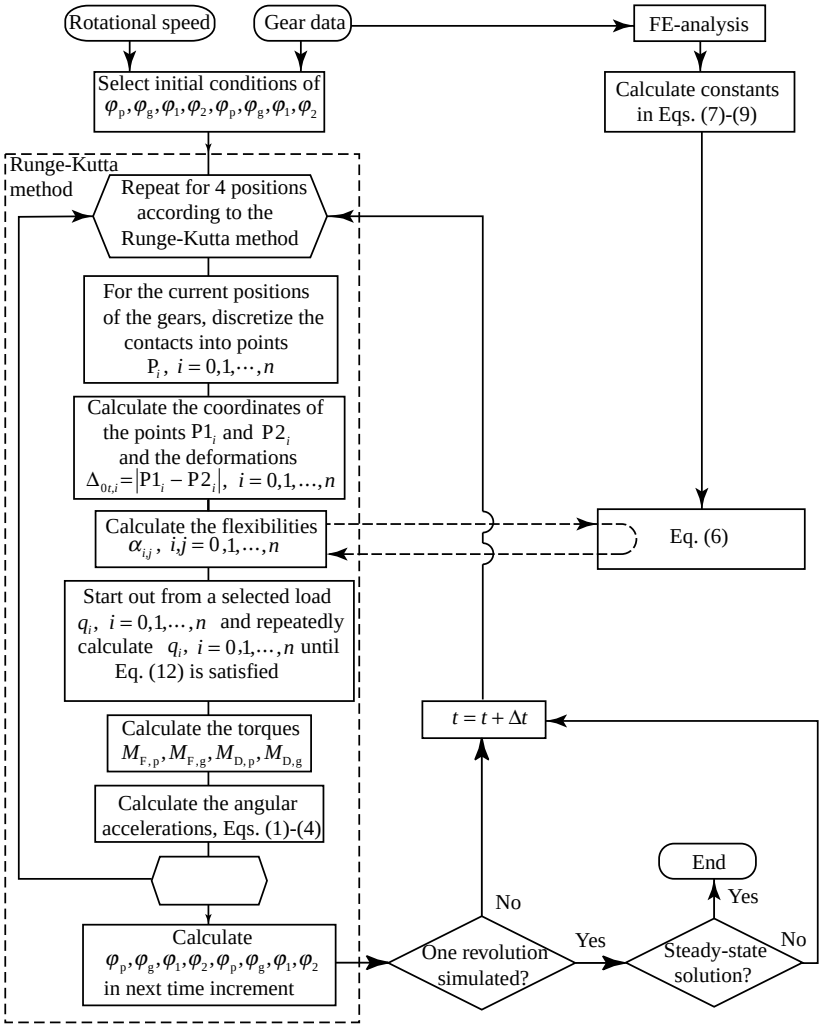

Fig. 8. Computational procedure.

As a result of the oscillations, the load distribution and thereby the contact pressure distribution will differ from the results obtained in the static analysis, cf. Fig. 7. This can be seen in Figs. 11–13 where the variation of the contact pressure along the face width and throughout the mesh is shown for three different rotational speeds. These figures are constructed in like manner as Fig. 7, but using the combinations of φ_p and φ_g from the dynamic steady state solution instead of the combinations that fulfil the static equilibrium condition. Figs. 11 and 12 show the contact pressure when running the gears at the third and the second resonances, respectively. In Fig. 13 the rotational speed is $\omega_p = 570$ rad/s in order to show the variation of the contact pressure near the main resonance speed. Here, in spite of the tip relief, the tip rounding comes into contact, which gives an excessive contact pressure due to the small radius of curvature of the tip rounding. In practice, such spikes will give a breakage of the tooth surfaces unless the edge is rapidly worn, which would result in a more reasonable contact pressure.

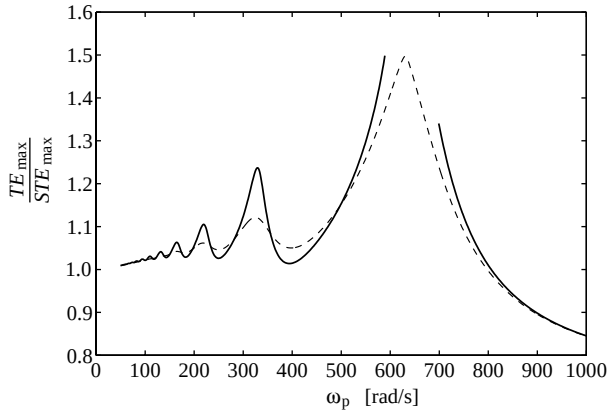

Fig. 9. Maximum transmission error: —, $d_{mesh} = 100$ Ns/m; - - -, $d_{mesh} = 200$ Ns/m.

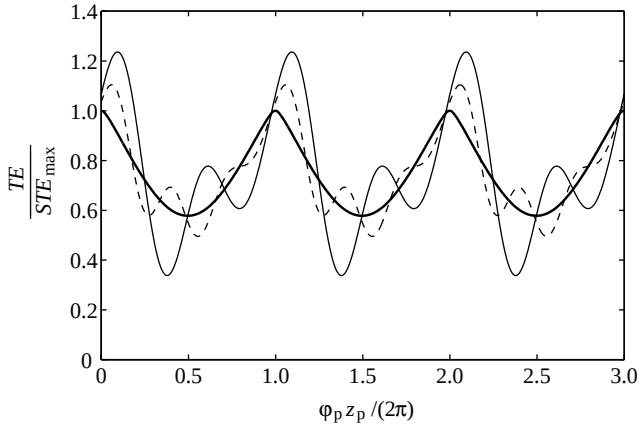

Fig. 10. Variation of the transmission error in steady-state, $d_{mesh} = 100$ Ns/m. —, $\omega_p = 330$ rad/s; - - -, $\omega_p = 220$ rad/s; ——, static solution.

7. Summary

The method described in the present paper makes it possible to predict the dynamic behaviour of a gear set, before it is manufactured. In addition, the method can be used in order to make parametrical studies of how the dynamic behaviour is affected by different design quantities such as the choice of the gear dimensions, the contact ratio or the amount of tip relief.

When a new tooth pair comes into mesh there is already at least one pair of teeth in the meshing region. Due to the deformation of the tooth pair(s) already in mesh, the two tooth flanks in the new contact initially touch each other at a point usually outside the plane of action. In this initial position, the two gear flanks have different velocities but the gears are undeformed and there is no load between the two mating gear teeth. An instant later the gears are slightly deformed, the point of contact has extended to a small area of contact and a small load arises between the gear teeth. Consequently, there is a continuous increase of the deformation and the load from zero at the beginning of the meshing. A corresponding situation is found at the end of the meshing where the

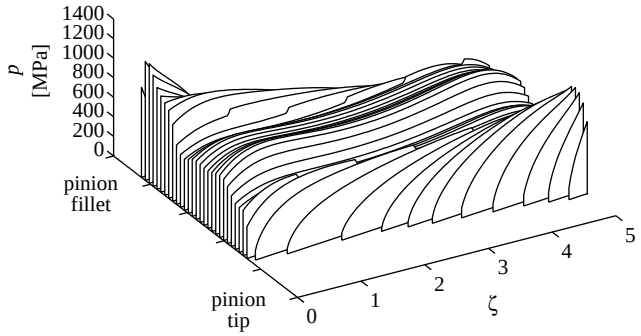

Fig. 11. Contact pressure, $\omega_p = 220\,\text{rad/s}$.

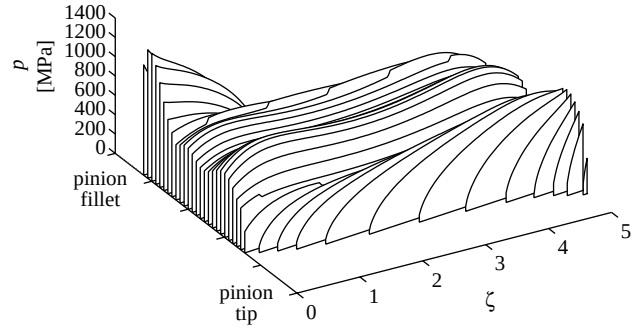

Fig. 12. Contact pressure, $\omega_p = 330\,\text{rad/s}$.

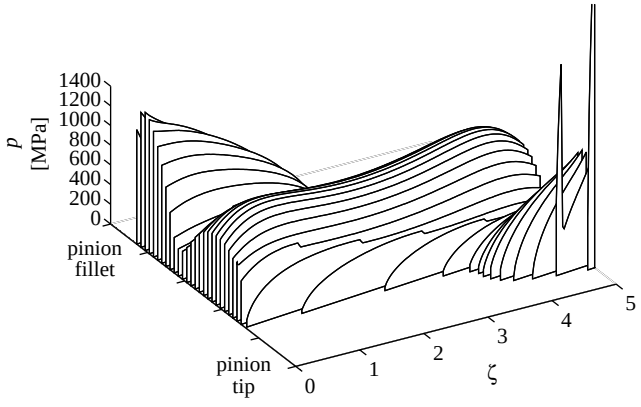

Fig. 13. Contact pressure, $\omega_p = 570\,\text{rad/s}$.

deformation and the load continuously decrease down to zero. To determine correctly the load variation during the mesh, especially at the beginning and at the end of the mesh, the model described in this paper calculates the position of the line of contact, which can be outside the plane

of contact, at every instant. To avoid the singularity which appears when the tip of one wheel makes contact with the gear flank of the other wheel, the connection between the tip relief and the tip surface is modelled by a circular arc instead of a sharp corner. Since the position of the line of contact is affected by the parts connected to the pinion and the gear, these parts have to be included in the analysis. In this work, they are represented by a one-degree-of-freedom system at each side of the gear set.

To determine the torque contributions from the gear contact, the deformation and the stiffness of the gears have to be analysed. Due to the oblique line of contact, the helical gear has to be modelled in three dimensions to accurately determine the deformation and thereby the tooth loads. In the present paper, a method comprising a combination of a finite element analysis and an analytical expression of the local contact deformation was used when analysing the deformation in order to calculate the load distribution along the line of contact. By adopting this method, the possibility of the finite element method to model the helical gear by its true geometry is utilised and yet the result of using an element mesh fine enough to make it possible to approximate the Hertzian load is avoided.

At some rotational speeds when the oscillations reach a certain level, the tip rounding comes into contact even if the gear teeth have a tip relief. With a smaller tip relief, the tip rounding comes into contact more often. Due to the small radius of curvature of the tip rounding, the contact pressure becomes excessive when the tip is in contact, which will lead to increasing wear of the gear tooth. This implies that, especially for gear teeth with a minor tip relief, the method presented in this report should gain by being combined with a model of the continuous wear of the gear teeth.

Acknowledgements

This work was supported by the Swedish Research Council for Engineering Sciences (TFR).

Appendix A. Nomenclature

E modulus of elasticity
J mass moment of inertia
L half contact width
M torque
b gear face width, ($b_0 = b/m_n$)
c torsional shaft stiffness
d damping coefficient
g base cylinder radius
h distance
m gear module
p contact pressure
q load intensity
s moment arm

u displacement
z number of teeth, axial co-ordinate
Δ distance
α influence function
α^* displacements from the FE-analysis
β helix angle
ζ non-dimensional axial co-ordinate, ($\zeta = z/m_n$)
v Poisson's ratio
ρ radius of curvature
τ, φ angular co-ordinate
ω_g, ω_p nominal rotational frequency

Subscripts
b beginning
c contact
e end
g gear
n normal
p pinion
1 driving side
2 driven side

References

[1] H.N. Özgüven, D.R. Houser, Mathematical models used in gear dynamics—a review, Journal of Sound and Vibration 121 (1988) 383–411.
[2] D.R. Houser, A. Seireg, An experimental investigation of dynamic factors in spur and helical gears, Journal of Engineering for Industry 92 (1970) 495–503.
[3] H. Matsuhisa, Y. Miyaji, S. Sato, Parametrically excited vibration with external constant load and damping, Memoirs of the Faculty of Engineering, Kyoto University 44 (1982) 158–167.
[4] K. Umezawa, T. Suzuki, T. Sato, Vibration of power transmission helical gears (Approximate equation of tooth stiffness), Bulletin of JSME 29 (1986) 1605–1611.
[5] Y. Cai, Simulation on the rotational vibration of helical gears in consideration of the tooth separation phenomenon (A new stiffness function of helical involute tooth pair), American Society of Mechanical Engineers Journal of Mechanical Design 117 (1995) 460–469.
[6] K. Umezawa, H. Houjoh, S. Matsumura, The influence of flank deviations on the vibration of a helical gear pair transmitting light load, International Power Transmission and Gearing Conference, American Society of Mechanical Engineers, DE-Vol. 43–2 (1992) 681–688.
[7] G.W. Blankenship, R. Singh, A new gear mesh interface dynamic model to predict multi-dimensional force coupling and excitation, Mechanism and Machine Theory 30 (1995) 43–57.
[8] G.W. Blankenship, R. Singh, Dynamic force transmissibility in helical gear pairs, Mechanism and Machine Theory 30 (1995) 323–339.
[9] A. Kahraman, Effect of axial vibrations on the dynamics of a helical gear pair, Journal of Vibration and Acoustics 115 (1993) 33–39.
[10] P. Velex, M. Maatar, A mathematical model for analyzing the influence of shape deviations and mounting errors on gear dynamic behavior, Journal of Sound and Vibration 191 (1996) 629–660.

[11] S. Honda, Rotational vibration of a helical gear pair with modified tooth surfaces (Modified tooth surface and its equivalent tooth profile), JSME International Journal Series C 36 (1993) 125–134.
[12] S. Honda, Rotational vibration of a helical gear pair with modified tooth surfaces (rotational motion of a gear pair and its dynamic increment of tooth load), JSME International Journal Series C 36 (1993) 375–385.
[13] S. Honda, Rotational vibration of a helical gear pair with modified tooth surfaces (verification of the new theory by experiment and a new design method for dynamic performance), JSME International Journal Series C 38 (1995) 112–121.
[14] L. Vedmar, On the Design of External Involute Helical Gears, Ph.D. Dissertation, Transactions of Machine Elements Division, Lund Technical University, Lund, 1981.
[15] C. Weber, K. Banaschek, Schriftenreihe Antriebstechnik, Ht. 11, Friedr. Vieweg, Braunschweig, 1953.